Microchemical Journal 162 (2021) 105825

Contents lists available at ScienceDirect

Microchemical Journal

journal homepage: www.elsevier.com/locate/microc

Electrochemical aptasensor of bisphenol A constructed based on 3D mesoporous structural SBA-15-Met with a thin layer of gold nanoparticles

Marzieh Nodehi [a], Mehdi Baghayeri [a,*], Roya Behazin [b], Hojat Veisi [c]

[a] Department of Chemistry, Faculty of Science, Hakim Sabzevari University, PO. Box 397, Sabzevar, Iran
[b] Department of Chemistry, University of Sistan and Baluchestan, P.O. Box 98135-674, Zahedan, Iran
[c] Department of Chemistry, Payame Noor University, 19395-4697 Tehran, Iran

ARTICLE INFO

Keywords:
Electrochemical aptasensor
Gold nanoparticles
Bisphenol A
Central composite design
Molecular docking
Response surface methodology

ABSTRACT

Herein, a simple and sensitive electrochemical aptasensor was fabricated on the electrodeposited nanoporous gold electrode. A layer of gold nanoparticle deposited on the surface of 3D mesoporous structures of SBA-15-Met provided a clean, stable, and biocompatible surface for self-assemble of chain BPA aptamers that bring about considerable advantages in both molecular recognition and signal enhancement. The most important factors affecting the design of the aptasensor, such as aptamer concentration, aptamer incubation time, BPA incubating time, and the pH of the solution, were optimized using a multivariate experiment design. For this purpose, a five-level central composite design and a response surface methodology were used. Under the optimized conditions, the proposed aptasensor exhibited a wide linear range from 10 to 1200 pM with an ultralow detection limit of 3.65 pM for BPA. According to molecular docking computational, some hydrogen bonds and the π-π interactions have led to a strong affinity between the aptamer and BPA molecules which causes the developed aptasensor to have high sensitivity and selectivity for BPA determination in food samples.

1. Introduction

Phenolic compounds have been identified as major priority pollutants by the United States Environmental Protection Agency and the European Union. These chemicals are known to be toxic and impose severe short and long-lasting effects on both humans and animals. They are carcinogens and cause harm to the red blood cells, even at low concentrations. Among the phenolic compounds, BPA is the most important synthetic compound with a production volume of over 3.8 million tons per year [1]. BPA is used in the production of polycarbonates and epoxy resins, and it can be present in various products for everyday use, including drinking water bottles, electronic equipment, thermal paper rolls, or toys [2]. BPA is also used in food contact materials, including canned food containers and food packaging that caused consumers to be exposed to BPA through food and drinking water. BPA is known as an endocrine-disrupting chemical as it mimics the function of natural hormones in the body by interacting with various biological receptors, such as estrogen receptor, thyroid hormone receptor, and androgen receptor [3]. Therefore, BPA hurts the reproductive system, immune system, nervous system, metabolic function, as well as for the growth and development of progeny [4]. Recent data suggested that there is a significant association between BPA levels in the body with the risk of obesity, diabetes, and heart disease [5]. Also, studies have shown that low levels of BPA in the body increased the risk of developing breast, prostate, and lung cancers [6]. Due to the harmful effects of BPA, the European Food Safety Authority has reduced the daily tolerance rate from 50 μg / kg body weight to 4 μg/kg body weight in 2015. Also, in 2008, Canada classified BPA as a toxic chemical and banned the use of BPA in baby bottles. Thereafter, the United States and some European countries, as well as some Asian countries, banned the

Abbreviations: SELEX, Systematic evolution of ligands by exponential enrichment; GCE, Glassy carbon electrode; ΔE_p, Peak to peak separation; EIS, Electrochemical impedance spectroscopy; CV, Cyclic voltammetry; DPV, Differential pulse voltammetry; FESEM, Field emission scanning electron microscope; TEM, Transition electron microscope; FT-IR, Fourier transform infrared spectroscopy; EDS, Energy dispersive x-ray spectroscopy; E, Estradiol; EE2, Ethinyl estradiol; Au NPs, Gold nanoparticles; GQDs, Graphen quantum dots; BPA, Bisphenol A; BPAF, Bisphenol AF; BPB, Bisphenol B; BPBP, Bisphenol BP; MCH, 6-Mercapto-1-hexanol; TCEP, Tris-(2-carboxyethyl) phosphine hydrochloride; DIEA, Diisopropylethylamine; CCD, Central composite design; Con. Aptamer, Aptamer concentration; t. Aptamer, Aptamer incubation time; t. BPA, BPA incubating time; R_{et}, Electron transfer resistance; RSD, Relative standard deviation.

* Corresponding author.
E-mail address: m.baghayeri@hsu.ac.ir (M. Baghayeri).

https://doi.org/10.1016/j.microc.2020.105825
Received 7 October 2020; Received in revised form 20 November 2020; Accepted 1 December 2020
Available online 3 December 2020

use of BPA [3]. Due to the various uses and releases of BPA in the surrounding environment, BPA is direct present in daily life. Therefore, the development of sensitive and reliable methods for the monitoring of trace amounts of BPA in the real samples is very important. The typical analytical techniques have been used for this purpose are chromatography methods [7], fluorescence [8], colorimetric aptasensor [1], chemiluminescence [9]. Nonetheless, these methods suffer from some limitations such as costly, need to the skilled operator, not portable, time-consuming, and requiring complex preparation [10]. Therefore, the development of novel methods for the determination of BPA seems necessary.

Aptamers are single-stranded DNA or short RNA sequences that synthesized from a synthetic oligonucleotide library using the automated method known as SELEX. Output aptamers from the SELEX process exhibit high selectivity and low detection limit, often in the nano and picomolar range [11–15]. The aptamers have received much attention due to their attractive properties and a special affinity to different targets such as pesticides [16], toxins [17], heavy metal ions [18], endocrine disruptors [19], and cells [20]. Aptamers are known as chemical antibodies and have broad advantages over antibodies, e.g. longer lifespan, cheap synthesis, easy to modify, and excellent thermal stability [21]. Also, aptamers are easy to be modified by different functional groups and labels, which stabilizes and immobilizes the aptamers on the surface of different nanoparticles [22]. Aptamer-based biosensors are called aptasensors. In the past few years, a variety of aptasensors have been fabricated mainly based on fluorescence [23], optical [24], and electrochemical [25] techniques. Amongst these techniques, the number of electrochemical aptasensors is continuously increasing due to the ease of integration of aptamers into electrochemical systems. Also, the ability to perform multiple analyses and rapid response are other features of electrochemical sensors [26]. Abnous et al. reported a novel electrochemical aptasensor based on nontarget-induced bridge assembly. They used a signal off method for BPA detection in $[Fe(CN)_6]^{3-}/^{4-}$ solution as a redox agent [27]. Kashefi-Kheyrabadi et al. fabricated an aptasensor based on the miniaturized gold electrode and ferrocene terminated anti aptamer of BPA. Upon addition of BPA, the BPA-aptamer complex is formed and ferrocene and BPA are close to the electrode surface, and direct oxidation signals of ferrocene and BPA are considered as analytical signals [28]. Yu et al. developed an electrochemical biosensor based on a single-stranded DNA-methylene blue complex for the determination of BPA. Under optimal conditions, a linear relationship was obtained with the logarithm of BPA concentrations in the range of 0.001–100 μg/L, and a detection limit of 0.4 ng/L was reported [29]. In recent years, our research team presented electrochemical aptasensors based on magnetic gold nanocomposite for BPA detection [30,31].

The first step in the fabrication of an aptasensor is to immobilize proper aptamer sequences on a conducting surface. Recently, modification of the electrode surface with nanomaterials such as multiwall carbon nanotubes [32], metal nanoparticles [33], conductive polymeric [34], and combinations of several kinds of nanostructures [35] has led to the development of highly sensitive aptasensors. Recently, Au NPs with unique properties such as large specific area, good biocompatibility, and excellent conductivity have been attracted considerable attention in the fabrication of electrochemical aptasensors [36,37]. Moreover, Au NPs can bind to the surface of many substrates through functional groups such as CN, NH_2, and SH. Therefore, aptamer chains with NH_2 or SH terminals can be easily immobilized on the surface of Au NPs [38]. The BPA electrochemical biosensors with specially designed anti-BPA aptamer and Au NPs not only can increase figures of merit of these biosensors but also provide a highly reproducible sensor for onsite use [39]. However, the major limitations of gold nanostructures are their poor adhesion to the substrate surface and complicated preparation procedure [40].

Au NPs loading on the surface of proper support makes them more stable and well dispersed. Shahamirifard et al. used zirconia NPs with chlorocholine chloride as a suitable substrate for the immobilization of Au NPs [41]. Tang et al. cast GQDs on the surface of GCE, and then Au NPs are well dispersed on the surface of GQDs electrochemically [42]. Razavipanah el al. prepared MWCNT-SiO_2@Au core–shell nanocomposite to fabricated BPA aptasensor. The Au NPs are well dispersed around the SiO_2 NPs and in a bed of MWCNT to provide sufficient stability at the GCE surface. Mesoporous silica would seem to be ideal support with the three-dimensional structure for metal nanoparticles [43]. Chen et al. immobilized Au NPs on the surface of TiO_2/SBA-15 nanocomposites and used as active plasmonic photocatalysts for the selective oxidation of aromatic alcohols [44].

In traditional experimental design methods (one variable at a time), only one factor is considered as a variable, and the other factors are at a constant level. In these methods, the interactions between variables are not studied. Also, many experiments are needed to do the research, which leads to increased time and cost. To overcome this problem, response surface methods have been proposed for optimization studies. These methods are a set of useful mathematical and statistical techniques for modeling and analyzing problems in which a reaction is influenced by several independent variables whose purpose is to optimize the response [45,46].

SBA-15 zeolite with owning high surface area, porosity, uniform pore size distributions, and biocompatibility have been used so far to make electrochemical biosensors, especially for determination glucose and hydrogen peroxide [47,48]. The novelty of this work is the use of metformin for SBA-15 functionalization. Metformin, with its NH and NH_2 groups, provide dendritic structures to immobilization of various metal nanoparticles on its surface. Also, Metformin use as a drug for the treatment of type 2 diabetes therefore, it is biocompatible with the human body and does not alter the structure of aptamers immobilized on its surface. Therefore, the use of SBA-15-Met can be used as a suitable substrate for aptamer immobilization to provide the electrochemical aptasensors. To our knowledge, no papers have been reported on the construction of aptasensor based on SBA-15-Met nanocomposite. On the other hand, although many studies have been performed on the detection of BPA using an aptasensor [11,25,28], no papers based on SBA-15-Met have been reported for the determination of BPA. For the first time, we have used SBA-15-Met nanocomposite as a suitable substrate for the fabrication of an electrochemical aptasensor for the determination of BPA.

In this work, an ultrasensitive and selective electrochemical aptasensor was developed on a self-supported SH-terminated anti-BPA aptamer and Au NPs. At first, the SBA-15/Met platform synthesized chemically to provide the proper substrate for Au NPs immobilization using a simple electrodeposition method. Integration of mesoporous silica and Au NPs created a large specific area with excellent stability and high conductivity to self-assembled SH-aptamer on it. The parameters affecting the aptasensor fabrication and the measurement conditions of BPA were investigated by CCD design combined with response surface methodology. The mechanism of BPA detection on the surface of the proposed aptasensor is the label-free strategy in $[Fe(CN)_6]^{3-}/^{4-}$ redox probe. The electrochemical behavior of the electrodes prepared at each step of the construction of the aptasensor and the final electrode in the presence and absence of BPA was investigated by cyclic voltammetry technique. The electrode showed a good linear response to changes in the BPA concentration in the 0.01–1.2 nM range. Molecular docking was done to find the interaction between the aptamer and the BPA molecules from the molecular point of view.

2. Experimental

The materials, instrumentation, synthesis process of SBA-15-Met, and real sample preparation are listed in the Supporting information.

2.1. Preparation of GCE/ SBA-15-Met/Au/aptamer/MCH electrode

Before preparing of GCE as a platform for the placement of the modifier and aptamer, the disulfide bonds in the anti-BPA aptamer removed by adding 2 mM reducing agent TCEP to the prepared aptamer solution in Tris-HCl 0.01 M (pH = 7.4). In the following, it was heated at 90 °C for 10 min and then placed in the refrigerator for 15 min at 4 °C. The surface of the GC electrode was polished with alumina slurry on a polishing cloth until a mirror-like surface was obtained. Then, it was rinsed separately with ethanol and double distilled water by sound waves for 2 min, and allowed to dry at room temperature. After that, 5 μL of SBA-15-Met nanocomposite, dispersed at ethanol 1.0 mg mL^{-1} was dropped onto the GCE surface and then allowed to dry at room temperature. The electrode prepared was called the GCE/SBA-15-Met. Au

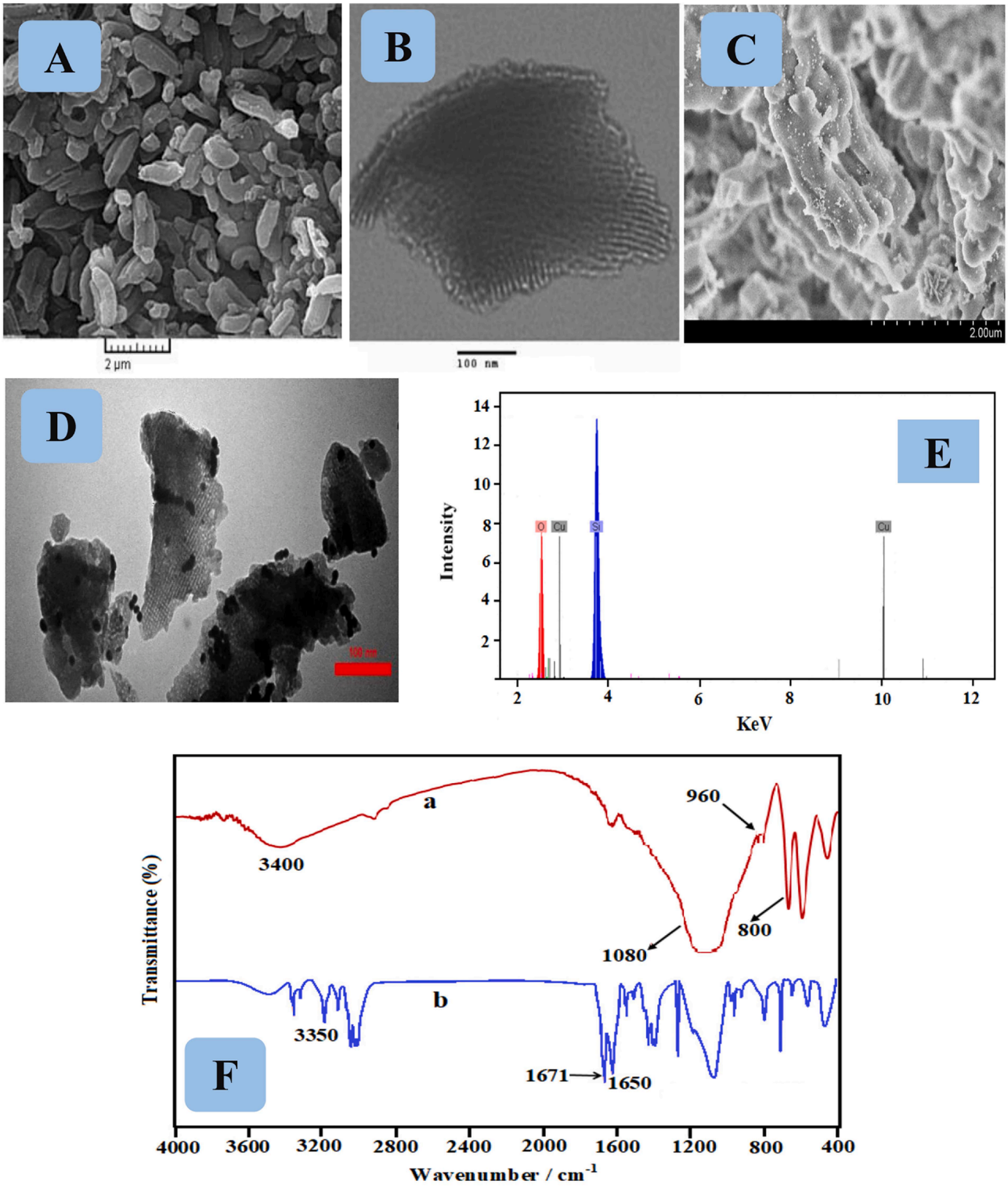

Fig. 1. (A) The FESEM and (B) the TEM images of SBA-15-Met. (C) The FESEM and (D) the TEM images of SBA-15-Met/Au nanocomposite. (E) The EDX pattern of SBA-15-Met. (F) The FT-IR spectra of SBA-15 (a) and SBA-15-Met nanocomposite (b).

NPs was deposited on the surface of GCE/SBA-15-Met electrode by cyclic voltammetry method (potential: −0.2 to +1.6 V vs. Ag/AgCl, number of cycle 25, scan rate 0.05 Vs^{-1}) in 6 mM $HAuCl_4$ solution. Then, 5 μL of the aptamer solution containing 2 mM TCEP and 1 μM aptamer in 10 mM Tris-HCl buffer solution (pH 7.6) was cast onto the obtained GCE/SBA-15-Met/Au electrode so that anti-BPA aptamer with -SH group at terminal assembles on Au NPs in the GC/SBA-15-Met/Au electrode. For aptamer immobilization, the modified electrode was placed in a 100% moisture-saturated environment for 16 h at 4 °C. After being washed with double distilled water to eliminate the unbound aptamer, 5 μL of 1 μM MCH was dropped onto the aptamer-immobilized GCE/SBA-15-Met/Au. The resulting mixture was incubated for 60 min to decrease the unspecific adsorption. Finally, the fabricated GCE/SBA-15-Met/Au/Apt electrode biosensor was rinsed with a 10 mM phosphate buffer solution (pH 7.6) and then, dried under N_2 stream.

For the detection of BPA, the fabricated biosensor was incubated into the binding buffer (25 mM Tris HCl, pH 9.65 with 100 mM NaCl, 10 mM $MgCl_2$, and 25 mM KCl) containing 0.9 nM of BPA for 55 min at room temperature. Then, electrochemical measurements were performed in 0.1 M KCl containing 5.0 mM $[Fe(CN)_6]^{3-/4-}$. The peak current change (ΔI) is defined by (i_0-i), where i is the anodic peak current of the aptasensor after BPA treatment, while i_0 is the initial anodic peak current without BPA. The preparation procedure of the GCE/SBA-15-Met/Au/Apt electrode is presented in Scheme S1.

3. Results and discussion

3.1. Characterization of SBA-15-Met/Au nanocomposite

The morphological features and component SBA-15-Met nanocomposite were investigated by FESEM, TEM, and, EDS analyzers. Moreover, the distribution of Au nanoparticles on the surface of GCE/SBA-15-Met was investigated by FESEM and TEM analyzer. The FESEM image of SBA-15-Met (Fig. 1A) shows the rod-like and the uniform channels of zeolite, while the channels are open along with the mesoporous particles. Also, it was revealed that the size of SBA-15-Met is about 400–1400 nm. Moreover, TEM image of the SBA-15-Met in Fig. 1B shows that the attachment of metformin to the SBA-15 zeolite has no distinct influence on the morphology of SBA-15. In the FESEM and TEM images of GCE/SBA-15-Met/Au, we can see the Au NPs distributed on the surface of GCE/SBA-15-Met that have spherical nanostructures with uniform size (Fig. 1C and D). According to EDS patterns of SBA-15-Met nanocomposite (see inset image of Fig. 1E), the strong peaks of Si and O illustrate that silicon and oxygen are the major elements in SBA-15-Met.

Fig. 1F illustrates the FT-IR spectra of SBA-15 (curve a) and SBA-15-Met (curve b). The peaks at 1080 and 800 cm^{-1} attributed to Si-O-Si and Si-O in SBA-15, respectively. Moreover, the peaks at 960 and 3400 cm^{-1} related to Si-OH groups. The FT-IR spectrum of SBA-15-Met exhibits the typical silica bands related to the main inorganic backbone of SBA. The clear band at 1052 cm^{-1}, which is attributed to Si-O-Si anti-symmetric stretching vibration, confirms the existence of a silica material. Moreover, signals that appeared at 3350 and 1650 cm^{-1} are related to the N–H stretching vibration and bending vibration of the amine group, respectively. The presence of bands in the spectral region of 1251 cm^{-1} can be attributed to the side-chain in-plane C—N—C and N—C—N bending of the triazine ring. The observed bands at 1671 and 1650 cm^{-1} corresponding to the C═NH and C═N—C stretching vibration [49]. These results indicate the successful functionalization of mesoporous SBA-15 material with triazine and metformin organic ligands.

3.2. Electrodepositon of Au NPs on the surface of GCE/SBA-15-Met

Fig. 2 shows the several successive voltammetric scans of Au NPs electrodeposition in a 0.5 M H_2SO_4 solution containing 0.6 mM $AuCl_4^-$ on the surface of GCE/SBA-15-Met. In the cyclic voltammograms was observed two reduction peaks, c_1 and c_2, and two oxidation peaks, a_1 and a_2. The c_1 and c_2 reduction peaks are related to the reduction of $AuCl_4^-$ to $AuCl_2^-$ and the further reduction of $AuCl_2^-$ to Au metal, respectively. The oxidation peaks indicated the reoxidation of Au electrodeposits. The area of the anodic peaks a_1 and a_2 are smaller than the area of reduction peaks that indicate Au electrodeposits cannot be completely reoxidized in each scan. Moreover, after the first scan, the Au^{3+} reduction peak shifted to more positive potentials implying that the formation of a gold layer on the electrode surface. The number of Au NPs deposited on the GCE/SBA-15-Met electrode increased with successive scans due to the continuous growth of the new pair of redox peaks (a_2/c_2). The anodic peak a_2 at 1.14 V appeared on the second scan and gradually increased with an increase in the number of scanning cycles, which represented the formation of Au oxides. On the reverse scan, the cathodic peak c_2 at 0. 90 V related to the reduction of the previously formed Au oxides.

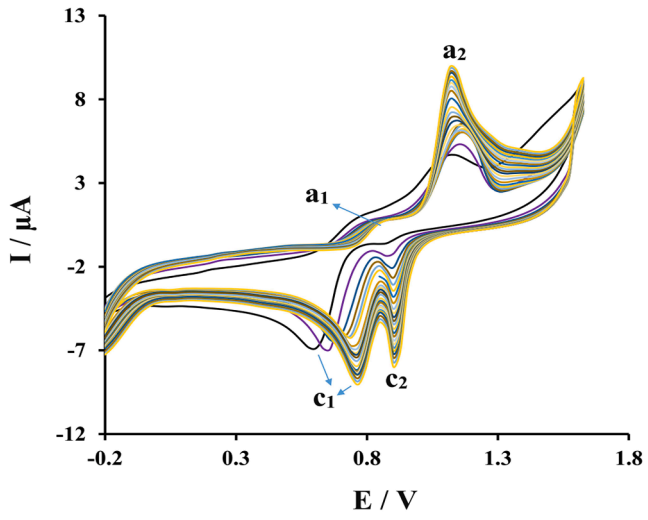

Fig. 2. Cyclic voltammograms of electrodeposition of Au NPs on the surface of GCE/SBA-15-Met in 0.5 M H_2SO_4 at scan rate 0.05 Vs^{-1}.

3.3. Aptasensor strategy

The sensing mechanism of BPA using the proposed aptasensor is based on the label-free strategy in the presence of $[Fe(CN)_6]^{3-/4-}$ as a redox mediator. The anti BPA aptamers with SH-terminate, self-assemble on the surface of Au NPs and provide long tunnels pathway for the electron transfer of $[Fe(CN)_6]^{3-/4-}$ ions. In the absence of BPA, the aptamers were remaining unfolded and the long tunnels are opened, therefore allow to the passage of electrons on the surface of electrode. But in the presence of BPA due to the interaction between aptamers with BPA molecules the conformation of aptamer was changed to G-quadruplex structure that closed the entrance of long tunnels. Therefore, the electron transfer process between the redox mediator and the electrode surface becomes difficult and causes the intensity of the electrochemical signal to decrease (Scheme S2).

3.4. Electrochemical properties of modified electrodes

Electrochemical characterization of fabricated aptasensor after each step was investigated by both CV and EIS in 0.1 M KCl containing 5.0 mM $[Fe(CN)_6]^{3-/4-}$ solution. Fig. 3A shows the cyclic voltammograms of various interfaces by plotting current signal vs. potential. The CV of bare GCE shows clear well defined reversible redox peaks corresponded to the $[Fe(CN)_6]^{3-/4-}$ redox probe with a ΔE_p of 325 mV. After GCE was modified with SBA-15-Met, the peak current decreased and ΔE_p increased to 400 mV. These results are likely to be related to the metformin functional groups and SBA-15 zeolite that limit the electron

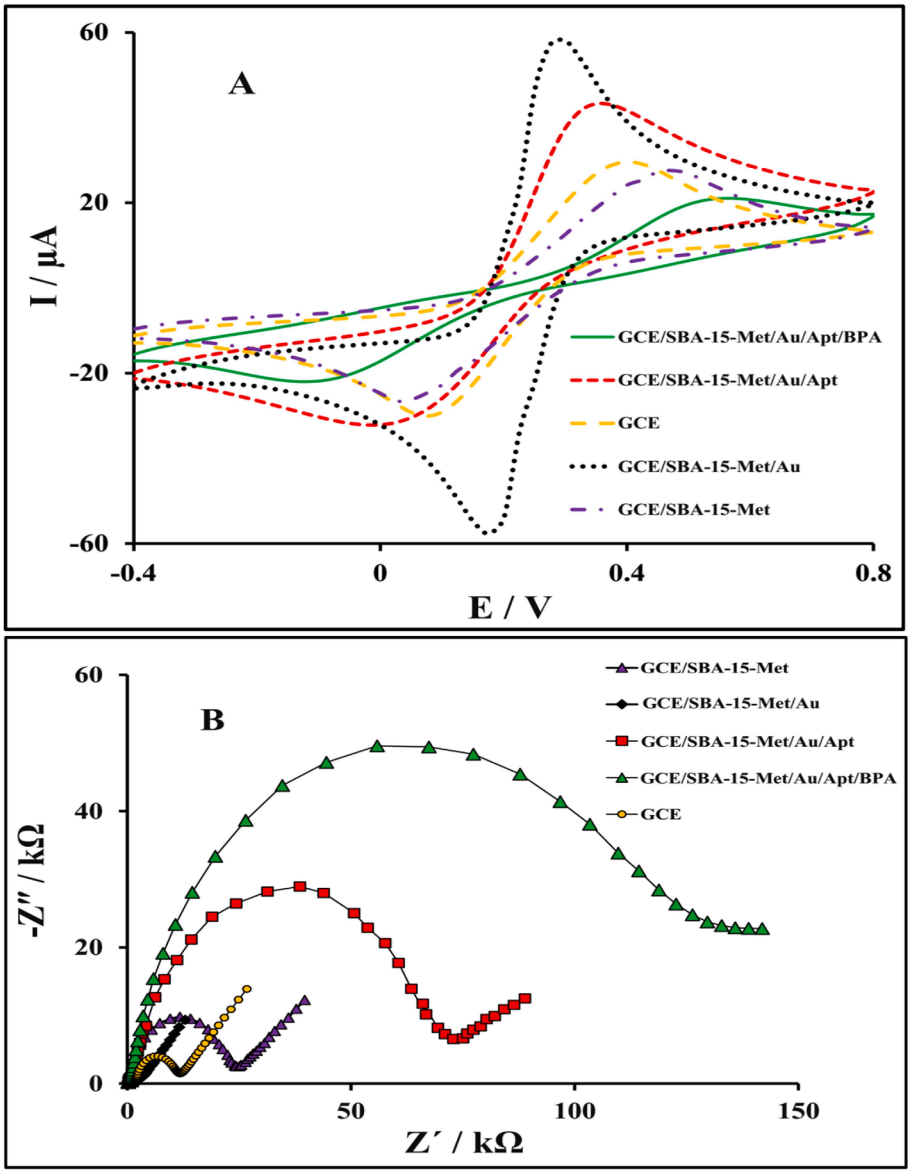

Fig. 3. (A) Cyclic voltammograms and (B) Nyquist plots of different modified electrode in 5 mM $Fe(CN)_6^{3-/4-}$ (1:1) solution containing 0.1 M KCl.

transport at the electrode surface. When GCE/SBA-15-Met was electrodeposited with Au NPs, the peak currents sharply increased and the reversible electrode process with ΔE_p 125 mV was observed. The presence of Au NPs with excellent conductivity significantly had enhanced the electron transfer kinetics on the surface of the electrode. Moreover, SBA-15-Met/Au was provided the proper substrate for the immobilization of aptamers by self-assembly. When the surface of the GCE/SBA-15-Met/Au was coated with anti-BPA aptamer and MCH, the redox peak experienced a clear fall in currents and an increase in the peak separation compared to the GCE/SBA-15-Met/Au electrode. These results confirm that the aptamers and MCH immobilized on the surface of GCE/SBA-15-Met/Au. The negative charge of aptamers leads to repulse redox ions of $[Fe(CN)_6]^{3-/4-}$ from the surface of the electrode. In the voltammogram of the GCE/SBA-15-Met/Au/Apt electrode incubated in 2.0 nM of BPA solution, the peak current decreased while the peak-to-peak separation potential increased. This finding can be accounted for by the fact that the formation of aptamer/BPA complexes could block the diffusion of $[Fe(CN)_6]^{3-/4-}$ towards the electrode surface.

For further evaluation of the steps taken for the modification of the aptasensor, the electrodes were also characterized by EIS. From the semicircle part of the Nyquist plot can be obtained information about the electrolyte resistance between the working and reference electrodes and R_{et} that affected by the diffusion of the ions from the electrolyte to the interface. As can be seen in Fig. 3B, the bare electrode possessed a R_{et} about 1200 Ω while R_{et} in the GCE modified with SBA-15-Met increased to 2400 Ω. When a layer of Au NPs electrodeposited on GCE/SBA-15-Met, R_{et} became smaller and shows nearly a line due to the good conductivity of Au NPs was desirable for electron transfer between the electrolyte and the interface. After the immobilization of aptamer and MCH on the surface of the modified electrode, the R_{et} value increased to 7500 Ω. These results indicate a strong interaction between the aptamers with SH terminates and Au NPs. Finally, when the aptasensor was incubated in 2.0 nM BPA for 55 min, a significant increase was observed in electron transfer resistance (R_{et} = 13589 Ω), proving the successful formation of aptamer/BPA complexes and the surface blocking for charge transfer of the redox system. These results are in line with that observed in the CV investigation.

3.5. Optimization of the performance of aptasensor

The influence of some parameters on the detection of BPA was optimized using a central composite design and results listed in

Supporting information.

3.6. Analytical performance of the electrochemical aptasensor

We investigated the analytical performances of the aptasensor through incubated GCE/ SBA-15-Met/Au/Apt in different concentrations of BPA with DPV. As shown in Fig. 4A, the peak currents decreased with increasing BPA concentrations, while ΔI increased in the range of 10–1200 pM. It can be explained that by increasing the concentration of BPA, the number of BPA-aptamer complexes increased, which prevented the electron transfer and decreased the peak current. A good linear relationship was obtained between the current change and BPA concentration (Inset of Fig. 4A). The regression equation was ΔI (μA) = 41.92 C_{BPA} (nM) + 7.585 with a correlation coefficient of 0.9904. The detection limit of 3.65 pM was obtained based on 3 S_b/m (S_b and m were the blank standard deviation and the slope of the linear curve). The quantification limit was 12.16 pM, which was calculated by 10 S_b/m. The analytical performance of the BPA aptasensor was compared with previously reported methods for BPA detection including fluorescence spectroscopy, HPLC-MS/MS, electrochemical immunosensors, electrochemical sensors, MIPs-based electrochemical sensor, and electrochemiluminescence aptasensors, the results were presented in Table 1. Although spectroscopy and analytical methods such as HPLC-MS and GC–MS methods are highly sensitive to the determination of BPA, the matrix effect in these methods is very high and requires complex pretreatment methods that are time-consuming and expensive. Therefore, most electrochemical techniques today, with advantages such as simplicity, low cost, and high sensitivity, are used to determination of BPA. Even among electrochemical sensors, the high toxicity of electrochemical immunosensors, preparation of imprinting material, and the removal of imprinting molecules in MIPs-based electrochemical sensors and low selectivity in electrochemical sensors cannot be ignored. Meanwhile, aptamer-based electrochemical sensors have excellent sensitivity and selectivity. As can be seen in Table 1, electrochemical aptasensors show better analytical performance for the determination of BPA compared to other methods and, in addition to their simplicity,

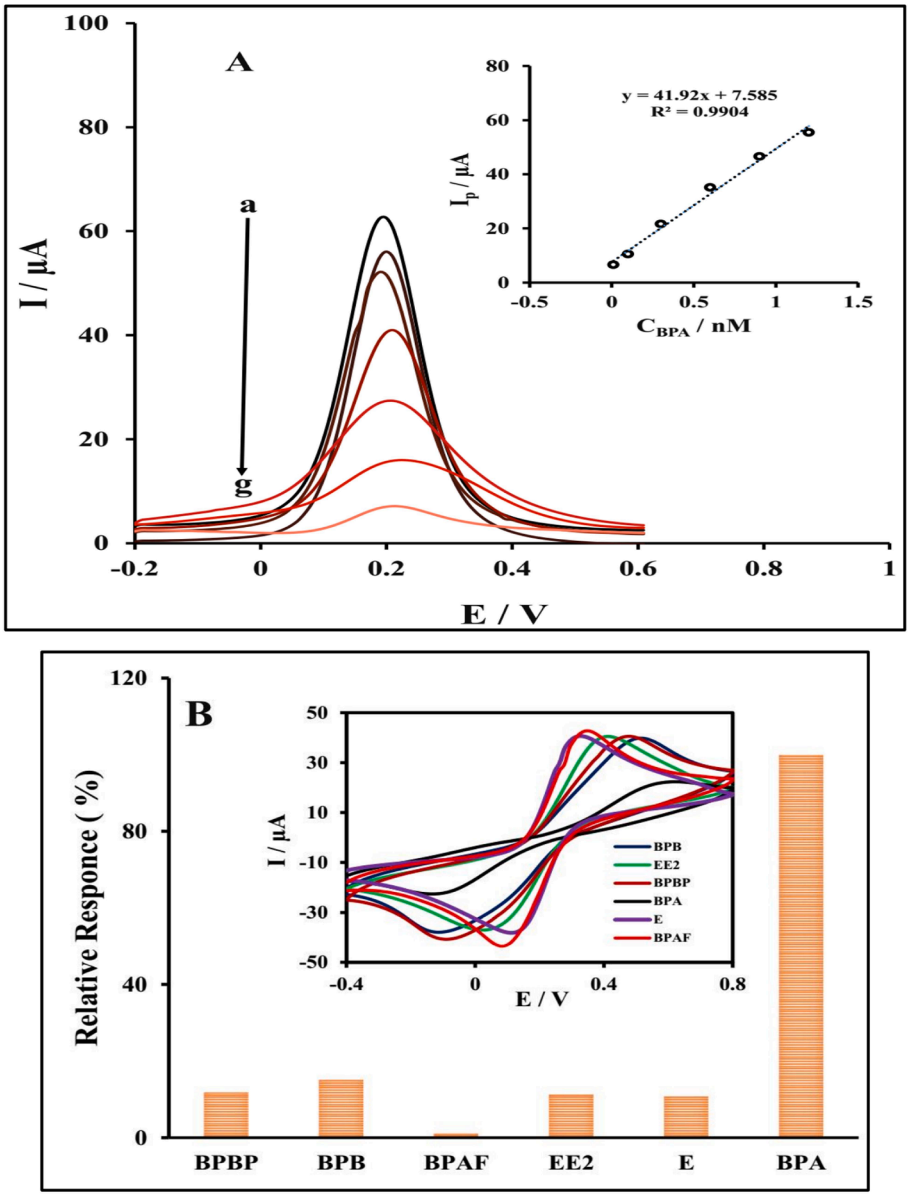

Fig. 4. (A) DPVs obtained at the GC/SBA-15-Met/Au/Apt electrode before (a) and after incubation in 0.01 (b), 0.1 (c), 0.3 (d), 0.7 (e), 0.9 (f) and 1.2 (g) nM of BPA solutions. Inset: linear dependence of the peak current change with BPA concentration. (B) Selectivity confirmation studies of the proposed aptasensor for determination of BPA.

Table 1
Comparison between various methods for determination of BPA with the proposed method.

Method	Modifier	LOD	LDR (nM)	Real sample	Ref.
Electrochemical aptasensor	Screen-printed gold electrode	15 pM	0.08–15	Tap water	27
Electrochemical aptasensor	MWCNT-SiO_2@Au	10 pM	0.1–100	Mineral water, orange juice milk	43
Electrochemical sensor	PtPd bimetallic nanoparticles and cationic pillar [5] arene decorated graphene	3.3 nM	$10–10^6$	Water and milk samples	[53]
Electrochemiluminescence aptasensor	Carbon nanodots composite as co-reaction of $Ru(bpy)_3^{2+}$ nanosheets	33 pM	$0.1–10^5$	Water samples	4
Electrochemical sensor	Molecularly imprinted polymer tailored on multiwalled carbon nanotubes	20 pM	$0.1–10^5$	Baby feeding bottle extracts	[54]
Excitation-emission matrix fluorescence	–	175 pM	–	PC plastics	[55]
HPLC–MS/MS	–	LOQ = 438 pM	–	Human plasma	[56]
Electrochemical immunosensor	Anti-BPA/AuNPs/MWCNTs/GCE	8700 pM	10–1000	Food fresh-keeping film	[57]
Electrochemical aptasensor	GCE/SBA-15-Met/Au /Apt	3.65 pM	0.01–1.2	Milk powder Fresh liquid milk	This work

have lower detection limits and wider linear range.

To research, the specificity of the electrochemical aptasensor, some potential substances, including BPB, BPAF, BPBP, E, and EE2, which had a similar function or similar structure with BPA were used as model interferents. Each time the GCE/SBA-15-Met/Au/Apt electrode was incubated in one of five interferents. The concentration of 0.9 nM and the DPV responses were recorded with the same method for determining BPA. The current change before and after the incubation of 0.9 nM of interferents was used to estimate the selectivity of the aptasensor. As shown in Fig. 4B, ΔI was about 21.07 μA in 0.9 nM BPA, whereas ΔI was less than 3.2 μA when the aptasensor was incubated in any one among five interferents. Overall caused by these interferents were less than 15.28% for that of BPA, indicating that the electrochemical aptasensor had good selectivity. This fact was mainly attributed to the high affinity of the aptamer to BPA. Also, the reproducibility and stability of the aptasensor were investigated. Its reproducibility was studied by detecting 0.9 nM BPA for five measurements by DPV under the same conditions. The RSD was 3.1%, this result represents an acceptable reproducibility. Furthermore, more than 95.8% of the original current response of the aptasensor remained after 10 days of storage at 4 °C, indicating the good stability of the aptasensor.

3.7. Real sample analysis

To investigate the applicability of electrochemical aptasensor in real samples, two milk samples, including liquid milk and milk powder, were analyzed by using the strategy established in this paper. The pasteurized liquid milk and milk powder were purchased from a local supermarket (Sabzevar, Iran). The examined milk samples were prepared as follows: 10.0 mL of liquid milk was mixed with 10.0 mL acetic acid (3%, v/v). After 30 min sonication, the mixture was centrifuged for 10 min at 10000 rpm. Then, the supernatant solution collected and added into a 50 mL volumetric flask and diluted with Tris-HCl buffer (pH 9.65). Finally, the prepared liquid milk sample was spiked with a defined BPA concentration. Moreover, the sample without adding BPA was used as a control group. In about milk powder, the preparation procedure was similar to the above processes except at first 5.0 g of milk powder was mixed with 5 mL of Tris-HCl buffer solution [30]. The result obtained was listed in Table 2. The recovery for BPA was between 95.4% and 104.2%, and the RSD results were smaller than 4.8%. These results displayed that the proposed aptasensor had acceptable sensitivity and accuracy in determining BPA in milk samples and had enormous potential in food applications.

Table 2
The results obtained for BPA detection in real sample (n = 5) using GCE/SBA-15-Met/Au/Apt electrode.

Sample	Added (nM)	Found (nM)	R.S.D	Recovery(%)
Fresh liquid milk	0	–	–	–
	0.1	0.104 ± 0.005	4.8	104.2
	0.5	0.477 ± 0.016	3.3	95.4
Milk powder	0	–	–	–
	0.1	0.100 ± 0.004	4.0	100.2
	0.5	0.509 ± 0.009	1.8	101.8

Milk powder and fresh liquid milk (Pegah, Iran Dairy Industries Co., Guilan, Iran).

3.8. Computational methods

The geometry optimization of BPA was carried out at the M06-2X/6–31 + G(d) level of theory [50] using the GAUSSIAN09 program package [51]. This compound docked into the aptamer and the binding energies were calculated using the genetic algorithm based on the Autodock 4.2 program package [52]. To obtain the tertiary structure of the aptamer molecules, a B-DNA composed of 63 nucleotides was designed and 100 ns MD simulations in water were applied to fold the structure using discovery Studio software.

According to Autodock, BPA and aptamer were prepared in the pdbqt format, and ligand considered flexible during the docking process. The search space was defined to encompass all aptamer structure as a box with dimensions of 65 Å × 65 Å × 65 Å manually. Autodock provides 10 predicted binding energy (ΔG_b values) and inhibition constant (K_i) from different docking poses, which the best $\Delta G_b = -4.45$ kcal mol^{-1} and K_i = 547.15 μM were considered as molecular docking score for docked BPA in aptamer (Fig. S2).

According to Fig. S2, some hydrogen bond interactions were observed between the NH group of G10 and C═O group of G52 nucleotides with OH groups of the BPA molecule. Also, the π-π interaction was formed between U nucleotide and BPA, in which these effective interactions demonstrated the ability of the BPA to bond to the aptamer molecule.

4. Conclusions

In summary, a new and label-free electrochemical aptasensor based on SBA-15 and Au NPs has been designed for the detection of BPA. The electrodeposition of Au NPs on the surface of SBA-15-Met improved the electrons transfer and the load amount of BPA aptamer by the self-assembly method that causes the enhancement of signal intensity and

improvement of detection sensitivity. The designed aptasensor showed excellent analytical performance with a detection limit of 3.65 pM and a linear range 10–1200 pM for the determination of BPA with high selectivity. Moreover, it has been successfully applied to detect BPA in real samples with satisfactory recovery between 95.4% and 104.2% with acceptable RSD. There will be great development potential in the analysis of food products. Also, the ability of interaction between BPA with aptamer was investigated using computational methods.

CRediT authorship contribution statement

Mehdi Baghayeri: Supervision, Conceptualization. **Marzieh Nodehi:** writing. **Roya Behazin:** software control . **Hojat Veisi:** review & editing.

Declaration of Competing Interest

The authors declare that they have no known competing financial interests or personal relationships that could have appeared to influence the work reported in this paper.

Acknowledgement

We would like to thank the post-graduate office of Hakim Sabzevari University for the support of this work.

Appendix A. Supplementary data

Supplementary data to this article can be found online at https://doi.org/10.1016/j.microc.2020.105825.

References

[1] E.H. Lee, S.K. Lee, M.J. Kim, S.W. Lee, Simple and rapid detection of bisphenol A using a gold nanoparticle-based colorimetric aptasensor, Food Chem. 287 (2019) 205–213.
[2] J. Michałowicz, Bisphenol A – Sources, toxicity and biotransformation, Environ. Toxicol. Pharmacol. 37 (2) (2014) 738–758.
[3] Y. Ma, H. Liu, J. Wu, L. Yuan, Y. Wang, X. Du, R. Wang, P.W. Marwa, P. Petlulu, X. Chen, H. Zhang, The adverse health effects of bisphenol A and related toxicity mechanisms, Environ. Res. 176 (2019) 108575–108585.
[4] X. Liu, L. Luo, L. Li, Z. Di, J. Zhang, T. You, An electrochemiluminescence aptasensor for analysis of bisphenol A based on carbon nanodots composite as co-reaction of $Ru(bpy)_3^{2+}$ nanosheets, Electrochim. Acta 319 (2019) 849–858.
[5] L. Caporossi, B. Papaleo, Bisphenol A and metabolic diseases: challenges for occupational medicine, Int. J. Environ. Res. Public Health 14 (9) (2017) 959.
[6] E. Mahmoudi, A. Hajian, M. Rezaei, A. Afkhami, A. Amine, H. Bagheri, A novel platform based on graphene nanoribbons/protein capped Au-Cu bimetallic nanoclusters: application to the sensitive electrochemical determination of bisphenol A, Microchem. J. 145 (2019) 242–251.
[7] T.A.V. Brigante, L.F.C. Miranda, I.D. de Souza, V.R. Acquaro Junior, M.E. C. Queiroz, Pipette tip dummy molecularly imprinted solid-phase extraction of Bisphenol A from urine samples and analysis by gas chromatography coupled to mass spectrometry, J. Chromatogr. B Analyt. Technol. Biomed Life Sci. 1067 (2017) 25–33.
[8] R. Mo, H. Liu, R. Lai, G. Deng, Z. Zhang, Z. Pei, H. Li, E. Xia, Ultrasound-assisted upper liquid microextraction coupled to molecular fluorescence for detection of bisphenol A in commercial beverages, Food Anal. Methods 10 (5) (2017) 1575–1581.
[9] M. Amjadi, J.L. Manzoori, T. Hallaj, A novel chemiluminescence method for determination of bisphenol A based on the carbon dot-enhanced HCO_3^-–H_2O_2 system, J. Lumin. 158 (2015) 160–164.
[10] P. Butmee, G. Tumcharern, P. Saejueng, D. Stankovic, A. Ortner, J. Jitcharoen, K. Kalcher, A. Samphao, A direct and sensitive electrochemical sensing platform based on ionic liquid functionalized graphene nanoplatelets for the detection of bisphenol A, J. Electroanal. Chem. 833 (2019) 370–379.
[11] R. Rapini, G. Marrazza, Electrochemical aptasensors for contaminants detection in food and environment: Recent advances, Bioelectrochemistry 118 (2017) 47–61.
[12] Z. Sun, Y. Hui Jin, X. Sun, R.G. Jiang, Mn-doping-induced hierarchical petal growth of flower-like 3D MOF assembled with black phosphorous nanosheets as an electrochemical aptasensor of human stress-induced phosphoprotein, Nanoscale 12 (2020) 14538–14548.
[13] Y. Sun, X. Jiang, H. Jin, R. Gui, Ketjen black/ferrocene dual-doped MOFs and aptamer-coupling gold nanoparticles used as a novel ratiometric electrochemical aptasensor for vanillin detection, Anal. Chim. Acta 1083 (2019) 101–109.
[14] H. Jin, R. Gui, X. Gao, Y. Sun, An amplified label-free electrochemical aptasensor of γ-interferon based on target-induced DNA strand transform of hairpin-to-linear conformation enabling simultaneous capture of redox probe and target, Biosens. Bioelectron. 145 (2019), 111732.
[15] Y. Sun1, H. Jin, X. Jiang, R. Gui, Black phosphorus nanosheets adhering to thionine-doped 2D MOF as a smart aptasensor enabling accurate capture and ratiometric electrochemical detection of target microRNA, Sens. Actuators B Chem. 309 (2020) 127777.
[16] D. Jiang, X. Du, Q. Liu, L. Zhou, L. Dai, J. Qian, K. Wang, Silver nanoparticles anchored on nitrogen-doped graphene as a novel electrochemical biosensing platform with enhanced sensitivity for aptamer-based pesticide assay, Analyst 140 (18) (2015) 6404–6411.
[17] A. Pfohl-Leszkowicz, R.A. Manderville, Ochratoxin A: an overview on toxicity and carcinogenicity in animals and humans, Mol. Nutr. Food Res. 51 (2007) 61–99.
[18] T. Bao, W. Wen, X. Zhang, Q. Xia, S. Wang, An exonuclease-assisted amplification electrochemical aptasensor for Hg^{2+} detection based on hybridization chain reaction, Biosens. Bioelectron. 70 (2015) 318–323.
[19] L. Shi, X. Rong, Y. Wang, S. Ding, W. Tang, High-performance and versatile electrochemical aptasensor based on self-supported nanoporous gold microelectrode and enzyme-induced signal amplification, Biosens. Bioelectron. 102 (2018) 41–48.
[20] S. Cai, M. Chen, M. Liu, W. He, Z. Liu, D. Wu, Y. Xia, H. Yang, J. Chen, A signal amplification electrochemical aptasensor for the detection of breast cancer cell via free-running DNA walker, Biosens. Bioelectron. 85 (2016) 184–189.
[21] D.P. Nikolelis, T. Varzakas, A. Erdem, G.P. Nikoleli, Portable Biosensing of Food Toxicants and Environmental Pollutants, CRC Press Taylor & Francis, London, 2013.
[22] S. Pang, T.P. Labuza, L. He, Development of a single aptamer-based surface enhanced Raman scattering method for rapid detection of multiple pesticides, Analyst 139 (8) (2014) 1895–1901.
[23] A.A. Goulko, F. Li, X. Chris Le, Bioanalytical applications of aptamer and molecular-beacon probes in fluorescence-affinity assays, Trends Analyt. Chem. 28 (7) (2009) 878–892.
[24] A.S. Sadeghi, N. Ansari, M. Ramezani, K. Abnous, M. Mohsenzadeh, S.M. Taghdisi, M. Alibolandi, Optical and electrochemical aptasensors for the detection of amphenicols, Biosens. Bioelectron. 118 (2018) 137–152.
[25] B. Deiminiat, G.H. Rounaghi, M.H. Arbab-Zavar, I. Razavipanah, A novel electrochemical aptasensor based on f-MWCNTs/AuNPs nanocomposite for label-free detection of bisphenol A, Sens. Actuat. B Chem. 242 (2017) 158–166.
[26] M. Velasco-Garcia, S. Missailidis, New trends in aptamer-based electrochemical biosensors, Gene Ther. Mol. Biol. 13 (2009) 1–10.
[27] K. Abnous, N.M. Danesh, M. Ramezani, M. Alibolandi, S.M. Taghdisi, A novel electrochemical sensor for bisphenol A detection based on nontarget-induced extension of aptamer length and formation of a physical barrier, Biosens. Bioelectron. 119 (2018) 204–208.
[28] L. Kashefi-Kheyrabadi, J. Kim, H. Gwak, K.A. Hyun, N.H. Bae, S.J. Lee, H. Jung, A microfluidic electrochemical aptasensor for enrichment and detection of bisphenol A, Biosens. Bioelectron. 117 (2018) 457–463.
[29] Z. Yu, Y. Luan, H. Li, W. Wang, X. Wang, Q. Zhang, A disposable electrochemical aptasensor using single-stranded DNA–methylene blue complex as signal-amplification platform for sensitive sensing of bisphenol A, Sens. Actuat. B Chem. 284 (2019) 73–80.
[30] M. Baghayeri, R. Ansari, M. Nodehi, I. Razavipanah, H. Veisi, Voltammetric aptasensor for bisphenol A based on the use of a MWCNT/Fe_3O_4@gold nanocomposite, Microchim. Acta 185 (7) (2018) 320–329.
[31] M. Baghayeri, R. Ansari, M. Nodehi, I. Razavipanah, H. Veisi, Label-free electrochemical bisphenol A aptasensor based on designing and fabrication of a magnetic gold nanocomposite, Electroanalysis 30 (9) (2018) 2160–2166.
[32] L. Hou, L. Jiang, Y. Song, Y. Ding, J. Zhang, X. Wu, D. Tang, Amperometric aptasensor for saxitoxin using a gold electrode modified with carbon nanotubes on a self-assembled monolayer, and methylene blue as an electrochemical indicator probe, Microchim. Acta 183 (6) (2016) 1971–1980.
[33] P. Luo, Y. Liu, Y. Xia, H. Xu, G. Xie, Aptamer biosensor for sensitive detection of toxin A of Clostridium difficile using gold nanoparticles synthesized by Bacillus stearothermophilus, Biosens. Bioelectron. 54 (2014) 217–221.
[34] R. Rapini, A. Cincinelli, G. Marrazza, Acetamiprid multidetection by disposable electrochemical DNA aptasensor, Talanta 161 (2016) 15–21.
[35] W. Xu, Y. Wang, S. Liu, J. Yu, H. Wang, J. Huang, A novel sandwich-type electrochemical aptasensor for sensitive detection of kanamycin based on GR-PANI and PAMAM-Au nanocomposites, New J. Chem. 38 (10) (2014) 4931–4937.
[36] T. Xiao, J. Huang, D. Wang, T. Meng, X. Yang, Au and Au-Based nanomaterials: Synthesis and recent progress in electrochemical sensor applications, Talanta 206 (2020), 120210.
[37] H. Jin, C. Zhao, R. Gui, X. Gao, Z. Wang, Reduced graphene oxide/nile blue/gold nanoparticles complex-modified glassy carbon electrode used as a sensitive and label-free aptasensor for ratiometric electrochemical sensing of dopamine, Anal. Chim. Acta 1025 (2018) 154–162.
[38] H.R. Akbari Hasanjani, K. Zarei, An electrochemical sensor for attomolar determination of mercury(II) using DNA/poly-L-methionine-gold nanoparticles/pencil graphite electrode, Biosens. Bioelectron. 128 (2019) 1–8.
[39] L. Zhou, J. Wang, D. Li, Y. Li, An electrochemical aptasensor based on gold nanoparticles dotted graphene modified glassy carbon electrode for label-free detection of bisphenol A in milk samples, Food Chem. 162 (2014) 34–40.
[40] G. Liu, C. Sun, D. Li, S. Song, B. Mao, C. Fan, Z. Tian, Gating of redox currents at gold nanoelectrodes via DNA hybridization, Adv. Mater. 22 (19) (2010) 2148–2150.

[41] S. Shahamirifard, Z. Razmia, S. Hajati, A simple ultrasensitive electrochemical sensor for simultaneous determination of gallic acid and uric acid in human urine and fruit juices based on zirconia-choline, Biosens. Bioelectron. 114 (2018) 30–36.
[42] J. Tang, R. Huang, S. Zheng, S. Jiang, H. Yu, Z. Li, J. Wang, A sensitive and selective electrochemical sensor based on graphene quantum dots/gold nanoparticles nanocomposite modified electrode for the determination of luteolin in peanut hulls, Microchem. J. 145 (2019) 899–907.
[43] I. Razavipanah, G. Rounaghi, B. Deiminiat, S. Damirchi, K. Abnous, M. Izadyar, M. Khavani, A new electrochemical aptasensor based on MWCNT-SiO_2@ Au core-shell nanocomposite for ultrasensitive detection of bisphenol A, Microchem. J. 146 (2019) 1054–1063.
[44] Y. Chen, W. Li, J. Wang, Q. Yang, Q. Hou, M. Ju, Gold nanoparticle-modified TiO_2/SBA-15 nanocomposites as active plasmonic photocatalysts for the selective oxidation of aromatic alcohols, RSC Adv. 6 (2016) 70352–70363.
[45] M.A. Armas, R. María-Hormigos, A. Cantalapiedra, M.J. Gismera, M.T. Sevilla, J. R. Procopio, Multiparametric optimization of a new high-sensitive and disposable mercury (II) electrochemical sensor, Anal. Chim. Acta 904 (2016) 76–82.
[46] A. Nezhadali, M. Mojarrab, Computational study and multivariate optimization of hydrochlorothiazide analysis using molecularly imprinted polymer electrochemical sensor based on carbon nanotube/polypyrrole film, Sens. Actuat. B Chem. 190 (2014) 829–837.
[47] Z. JingJing, Z. JunJie, A novel amperometric biosensor based on gold nanoparticles-mesoporous silica composite for biosensing glucose, Sci. China Ser B-Chem. 52 (2009) 815–820.
[48] M. Hasanzadeh, N. Shadjou, M. Guardia, M. Eskandani, P. Sheikhzadeh, Mesoporous silica-based materials for use in biosensors, Trends Anal. Chem. 33 (2012) 117–129.
[49] H. Veisi, M. Hamelian, S. Hemmati, A. Dalvand, CuI catalyst heterogenized on melamine-pyridines immobilized SBA-15: heterogeneous and recyclable nanocatalyst for Ullmann-type CAN coupling reactions, Tetrahedron Lett. 58 (2017) 4440–4446.
[50] Y. Zhao, N.E. Schultz, D.G.J. Truhlar, Design of density functionals by combining the method of constraint satisfaction with parametrization for thermochemistry, thermochemical kinetics, and noncovalent interactions, J. Chem. Theory Comput. Chem. Theory Comput. 2 (2) (2006) 364–382.
[51] M.J. Frisch, G.W. Trucks, H.B. Schlegel, G.E. Scuseria, M.A. Robb J.R. Cheeseman, Gaussian 09, Revision A.02, Gaussian Inc. Wallingford CT, (2009).
[52] G.M. Morris, H. Ruth, W. Lindstrom, M.F. Sanner, R.K. Belew, D.S. Goodsell, A. J. Olson, Software news and updates AutoDock4 and AutoDockTools4: automated docking with selective receptor flexibility, J. Comput. Chem. 30 (16) (2009) 2785–2791.
[53] H. Liang, Y. Zhao, H. Ye, C.J. Li, Ultrasensitive and ultrawide range electrochemical determination of bisphenol A based on PtPd bimetallic nanoparticles and cationic pillar[5] arene decorated graphene, Electroanal. Chem. 855 (2019), 113487.
[54] T.S. Anirudhan, V.S. Athira, V. Chithra Sekhar, Electrochemical sensing and nano molar level detection of Bisphenol-A with molecularly imprinted polymer tailored on multiwalled carbon nanotubes, Polymer 146 (2018) 312–320.
[55] Y. Chen, H. Wu, X. Sun, T. Wang, H. Fang, Y. Chang, L. Cheng, Y. Ding, R. Yu, Simultaneous and fast determination of bisphenol A and diphenyl carbonate in polycarbonate plastics by using excitation-emission matrix fluorescence couples with second-order calibration method, Spectrochim. Acta A Mol. Biomol. Spectrosc. 216 (2019) 283–289.
[56] G. Cambien, N. Venisse, V. Migeot, S. Rabouan, M. Belmouaz, G. Binson, M. Albouy-llaty, S. Ayraudthevenot, A. Dupuis, Simultaneous determination of bisphenol A and its chlorinated derivatives in human plasma: sevelopment, validation and application of a UHPLC–MS/MS method, Chemosphere 242 (2020), 125236.
[57] Y. Huang, X. Li, S. Zheng, A novel and label-free immunosensor for bisphenol A using rutin as the redox probe, Talanta 160 (2016) 241–246.